

Magnetic and resonance properties of crystalline and amorphous CuGeO_3

G. A. Petrakovskii, K. A. Sablina, A. M. Vorotynov, A. I. Kruglik, A. G. Klimenko, A. D. Balayev, and S. S. Aplesnin

L. V. Kirenski Institute of Physics, Academy of Sciences of the USSR, Siberian Branch

(Submitted 30 January 1990)

Zh. Eksp. Teor. Fiz. **98**, 1382–1389 (October 1990)

We report results of a comprehensive study of the magnetic properties in crystalline and amorphous CuGeO_3 which we synthesized. We use the Monte Carlo method to interpret experimental data. We determine the magnetic structure of crystalline CuGeO_3 for $T < T_N$ in the framework of the model used. We estimate the magnitudes of the exchange integrals and show that the magnetic properties of the crystalline and amorphous material differ sharply.

1. INTRODUCTION

A study of the effect of amorphization on the magnetic properties of a crystal is specially useful when comparisons between the magnetic properties of the amorphous and crystalline states of a given material are possible. It has been predicted that the amorphization of magnetic materials with an anisotropic distribution of exchange interactions can change the type of magnetic order and alter the values of the temperature of the magnetic phase transition considerably; in particular, the transition temperature can increase.^{1–3} A search for crystals which exhibit these properties and which go into the amorphous state upon rapid quenching from the melt has followed these predictions.

Up to now, several amorphous compounds which follow the theoretical predictions have been obtained.^{4–6} For further studies of amorphization effects in magnetic materials, we chose the AGeO_3 ($A = \text{Co}, \text{Mn}, \text{Fe}$) class of compounds with a pyroxene structure and antiferromagnetic order. It has been shown that these compounds can be easily obtained in the amorphous state and that they are spin glasses.⁷

In the present work, we study structure, resonance and magnetic properties of crystalline and amorphous CuGeO_3 .

2. SAMPLE PREPARATION

Polycrystalline CuGeO_3 samples were synthesized by a ceramic technology. The growth process was repeated three times. Single crystals were grown from the melt of a mixture of GeO_2 and CuO with a 1:1.2 ratio, respectively. The melt, placed in a platinum crucible, was cooled slowly from 1200 °C. The crystals obtained were transparent and blue in color. The largest dimensions of the prisms were $5 \times 3 \times 3 \text{ mm}^3$. The crystals cleave easily along layers in the bc plane.

The amorphous material was obtained using a catapult furnace.⁴ Polycrystalline samples were melted. The rate of quenching was 10^6 deg/sec . Shining bent black plates with typical dimensions of $30 \times 10 \times 0.1 \text{ mm}^3$ were obtained by the amorphization process. All samples were checked by x-ray analysis.

Nonequilibrium is the distinguishing feature of the amorphous state. It is clearly seen in amorphous CuGeO_3 by differential thermal analysis (DTA). Figure 1 shows thermograms for amorphous and crystalline samples. The exothermal peak observed at 637 °C on curve 1 is typical of crystallization of amorphous states. The DTA data for crystalline CuGeO_3 (curve 3) as well as the thermogram of amorphous CuGeO_3 (curve 2) do not reveal thermal anomalies

in the temperature range from 550 to 800 °C. It is interesting to note that black amorphous samples turn out green in color after crystallization at 637 °C.

X-ray patterns of the quenched CuGeO_3 melt obtained with a DRON-2 apparatus (CuK_α radiation) reveal diffuse scattering which therefore confirms that the material is indeed amorphous. Electrical measurements performed at temperatures of 4.2 K to 300 K show that amorphous CuGeO_3 is insulating with a resistivity $\rho_{300 \text{ K}} \sim 10^{10} \Omega \cdot \text{cm}$.

3. CRYSTAL STRUCTURE

Polycrystalline and single crystal CuGeO_3 samples were studied by x-rays (CuK_α radiation and Laue method, respectively). The crystal symmetry and parameters of the unit cell determined are in agreement with the data of Ref. 8. According to the data of Ref. 8, CuGeO_3 belongs to the polar space group $\text{Pb}2_{1m}$ (C_{2v}^2) with primitive cell parameters $a = 4.793 \text{ \AA}$, $b = 8.503 \text{ \AA}$, and $c = 2.942 \text{ \AA}$. There are two formula units in the primitive cell. Simple GeO_3 chains, with a repeating period of one tetrahedron along the c axis (Fig. 2), are typical of this compound. Cu atoms lie on octahedral sites between tetrahedral chains. The octahedra are also connected in chains sharing edges along the c axis and vertices along the b axis. Therefore, two-dimensional layers in cb planes are made up of octahedra. Below, we give (see Fig. 2) interatomic distances r (in units of Å) and angles φ (in units of deg) for different orientations of the CuGeO_3 crystal:

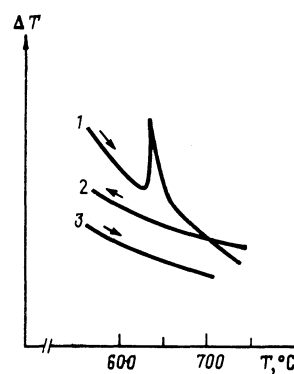


FIG. 1. Thermograms of amorphous and crystalline CuGeO_3 : 1—amorphous sample heated at a rate of 4.5 deg/min; 2—amorphous sample cooled after heating to 950 °C; 3—crystalline sample heated at a rate of 4.5 deg/min.

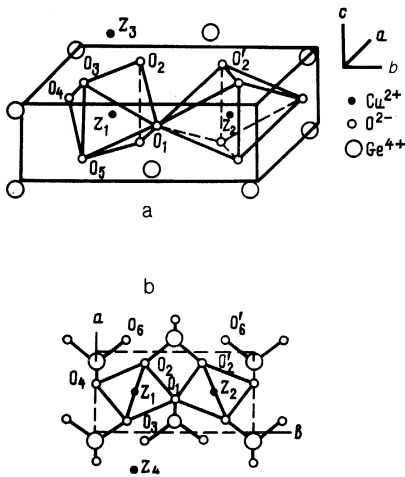


FIG. 2. Crystal structure of CuGeO_3 (not all Ge atoms are shown in part a).

r	Z_1-O_1	Z_1-O_2	Z_1-O_3	Z_1-Z_2	Z_1-Z_3
	2,32	2,23	2,23	4,25	2,942
r	O_2-O_2'	O_2-O_6	Z_1-Z_4	O_2-O_3	O_3-O_5
	2,60	2,48	4,793	3,38	2,942
φ	$Z_1-O_1-Z_2$	$Z_1-O_2-Z_3$	$O_2-Z_1-O_3$	$Z_1-O_1-O_2'$	
	132	82	98	114	

The octahedra and tetrahedra are strongly distorted. For example, some O–O distances in the tetrahedra are of 2.60 Å, whereas their average value is 2.97 Å. Another anomaly of the CuGeO_3 structure is the unusually small distance (2.48 Å) between oxygen O_2 and O_6 atoms in adjacent chains. We note that the ionic radius of O^{2-} is equal to 1.36 Å.⁹ Such short oxygen–oxygen distances are not observed in other AGeO_3 ($A = \text{Mn, Co, Fe}$) type compounds. Furthermore, in contrast with these compounds the GeO_3 chains in CuGeO_3 are strongly elongated and the Cu atoms lie on crystallographically equivalent sites. Using the atomic positions given in Ref. 8, it is easy to check (see Fig. 2) that the arrangement of atomic centers of mass is symmetric. The inversion centers coincide with the Cu atomic sites. This, in our opinion, contradicts the conclusions of Ref. 8 on the polar character of CuGeO_3 .

Measurements of the temperature variation of lattice constants do not reveal any structural phase transitions between 300 K and 1000 K. Electrical measurements for temperatures of 4.2 K–630 K show that CuGeO_3 is insulating and that $\rho_{300\text{K}} \sim 10^{13} \Omega \cdot \text{cm}$.

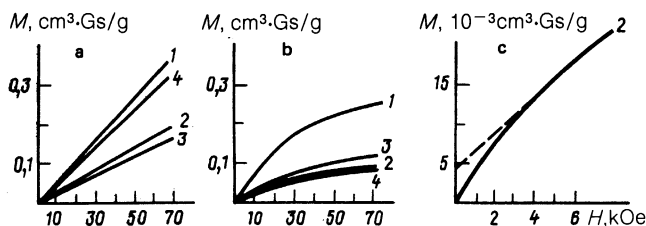


FIG. 3. Magnetization of the CuGeO_3 crystal for three crystallographic axes at different temperatures: a— $T = 8$ K; b— $T = 2$ K; c— $T = 4$ K. Curves 1, 2, and 3 correspond to the magnetic field parallel to the a, b, and c crystal axes, respectively; curve 4 is calculated by the Monte Carlo method for temperatures above and below the Néel temperature ($T_N = 7$ K). The dashed curve in part c shows the spontaneous magnetic moment M along the b crystal axis.

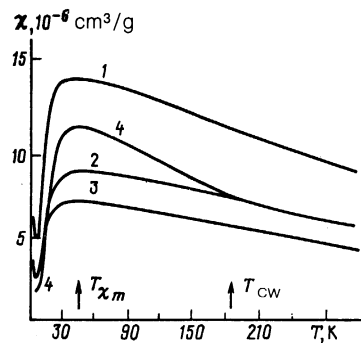


FIG. 4. Susceptibility of the CuGeO_3 crystal for three crystallographic axes. Curves 1, 2, and 3 correspond to the susceptibility along the a, b, and c crystal axes, respectively; curve 4 is calculated by the Monte Carlo method. The temperature of maximum of susceptibility, $T_{\chi m}$, and the temperature T_{cW} , where the susceptibility departs from the Curie-Weiss law, are shown by arrows.

4. MAGNETIC PROPERTIES

An automated vibrating magnetometer was used to measure the static magnetic properties of a CuGeO_3 crystal in fields of up to 80 kOe at temperatures of 2 K–300 K. Figure 3 shows results of magnetization measurements along three crystallographic axes. At low temperatures, a spontaneous magnetic moment M is observed. Its magnitude decreases as the temperature increases. The spontaneous magnetic moment M is oriented along the b crystal axis. For $T < 8$ K, the field dependence of the magnetization is nonlinear.

We have to note that the neutron diffraction patterns (for $\lambda = 1.71$ Å and $\lambda = 2.41$ Å) obtained for CuGeO_3 powder at $T = 4.2$ K and $T = 293$ K are identical. Therefore, our attempt to observe changes in the type of magnetic structure was unsuccessful. However, hysteresis loops were observed in the CuGeO_3 powder at $T = 4$ K.

The magnetic susceptibility of polycrystalline and amorphous samples was measured using a SQUID magnetometer in fields of 1.2 Oe at temperatures of 2 K–80 K. For single-crystal samples we used magnetization data obtained on the vibrating magnetometer. The experimental results for single crystals are exhibited in Fig. 4. The susceptibility is anisotropic up to room temperature. A minimum and subsequent sharp rise of the susceptibility for $T < 7$ K is related to the appearance of a spontaneous magnetic moment and determines the Néel temperature.

Since the range of temperatures in which the inverse

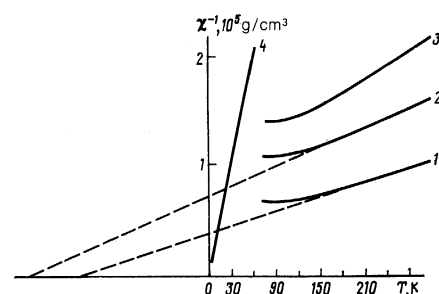


FIG. 5. Dependence of the inverse susceptibility on temperature for crystalline CuGeO_3 . Curve notation is the same as in Fig. 4. Curve 4 shows the dependence of the inverse susceptibility on temperature for amorphous CuGeO_3 .

susceptibility is linear is small (see Fig. 5), there is a large error in the determination of the paramagnetic Néel temperature Θ . We obtained $\Theta_b = (-250 \pm 15)$ K, $\Theta_a = (-180 \pm 20)$ K, $\Theta_c = (-180 \pm 70)$ K for Θ along the **b**, **a**, and **c** axis, respectively. The effective magnetic moment, μ_{eff} , and the paramagnetic Néel temperature, Θ , obtained from the temperature dependence of the susceptibility in polycrystalline CuGeO_3 are $2.19 \mu_B$ and -200 K, respectively. Measurements for amorphous CuGeO_3 show that the susceptibility is paramagnetic in the temperature range of 2 K–80 K. We obtained $\Theta = -1.3$ K, $C = 3.09 \cdot 10^{-4} \text{ cm}^3 \cdot \text{K}/\text{g}$ (C is the Curie constant) and $\mu_{\text{eff}} = 0.7 \mu_B$. Therefore, the amorphization process leads to drastic changes in the magnetic properties of crystalline systems.

5. RESONANCE PROPERTIES

Resonance measurements were carried out using a RE-1307 EPR spectrometer at a frequency of 9.4 GHz for temperatures of 4 K–300 K. The variations of the line width, ΔH , and of the resonant field, H_R , with temperature and sample orientation were studied using electron paramagnetic resonance. Figure 6 shows the temperature dependence of ΔH for magnetic fields along the **a**, **b**, and **c** crystallographic axes. The $\Delta H(T)$ dependence is linear in the 30 K–300 K range. The temperature variation of the resonant field H_R is shown in Fig. 7. H_R depends weakly on temperature along all crystal axes. The g -factor for $\mathbf{H} \parallel \mathbf{a}$, $\mathbf{H} \parallel \mathbf{b}$, and $\mathbf{H} \parallel \mathbf{c}$ is equal to 2.19, 2.266, and 2.083, respectively, at room temperature. Figure 8 shows the angular dependence of ΔH at room temperature. The amorphization process leads to significant changes in the resonance properties of CuGeO_3 (see Fig. 6). At room temperature, the line width, ΔH , becomes three times smaller than the line width in the crystalline sample. The temperature behavior of ΔH is qualitatively different: ΔH increases monotonically and slowly as the temperature decreases. The resonant field is independent of temperature in the 80 K–300 K range; it decreases below 80 K.

6. DISCUSSION

The results of magnetization measurements (Fig. 3) and EPR data (Fig. 6) show that magnetic long-range order exists in the CuGeO_3 system below 7 K. Anisotropy of the magnetic properties (susceptibility) persists for $T > T_N = 7$ K. Analysis of the crystal structure and of the angles at which the Cu–O–Cu exchange interaction takes place (see above) indicates that the CuGeO_3 magnetic system is on a plane. The magnetic layers lie in the bc plane.

Quantitative analysis of the exchange interactions by

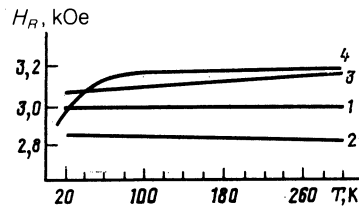


FIG. 7. Variation of the resonance EPR field with temperature. Curve notation is the same as in Fig. 6.

the Gudenaf's method allows us to assign the signs and relative magnitudes of the exchange interactions in the crystal. The exchange interaction along the **c** axis fulfills $J_1 > 0$, whereas the exchange interaction along the **b** axis obeys $J_0 < 0$ and $|J_0| > |J_1|$. The different values obtained for the paramagnetic Néel temperature for three crystallographic orientations (see Fig. 5) indicate that the exchange interaction is anisotropic in the system studied. To interpret the susceptibility measurements, we use the Monte Carlo method. We simulate the magnetic state of a Heisenberg system with classical spins on a 40×40 spin lattice on a plane. We also take into account next-nearest-neighbor interactions in the bc plane: $J_2 > 0$ and $|J_0| > |J_1| > |J_2|$. The system Hamiltonian is

$$\mathcal{H} = \sum_{ij} (J_0^{zz} S_i^z S_j^z + J_0^{xx} S_i^x S_j^x + J_0^{yy} S_i^y S_j^y) + \sum_{ik} J_1 S_i S_k + \sum_{il} J_2 S_i S_l + \sum_i \mathbf{H} S_i, \quad (1)$$

where S_i are the spins of Cu^{2+} ions.

The resulting variation of the magnetization $M(H)$ with field and variation of the susceptibility $\chi(T)$ with temperature are shown in Figs. 3 and 4, respectively. They follow qualitatively the experimental behavior of $M(H)$ and of $\chi(T)$. An important result of our model is the existence of a weak spontaneous magnetic moment. It appears when a ferromagnetic bond $J_2 = 0.5J_1$, which is frustrated for $J_0 < 0$ and $J_1 > 0$, is introduced into Hamiltonian (1). Figure 9 exhibits variations of the spontaneous moment $M(T)$ and of the Néel temperature $T_N(H)$ calculated by the Monte Carlo method.

Comparison of calculated and experimental results shows qualitative agreement. It is interesting to note that the calculated spontaneous moment, shown in Fig. 9a, vanishes as $T \rightarrow 0$. Therefore, the spontaneous magnetic moment M is induced by finite temperature. The physics of this phenomenon can be understood by considering the thermal oscillations of spins. At $T = 0$ the magnetic structure is collinear.

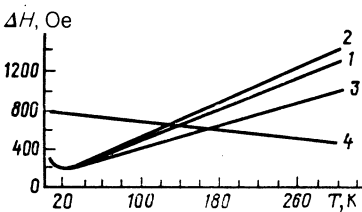


FIG. 6. Variation of the EPR line width with temperature for crystalline and amorphous CuGeO_3 : 1— $\mathbf{H} \parallel \mathbf{a}$; 2— $\mathbf{H} \parallel \mathbf{b}$; 3— $\mathbf{H} \parallel \mathbf{c}$; 4—amorphous sample.

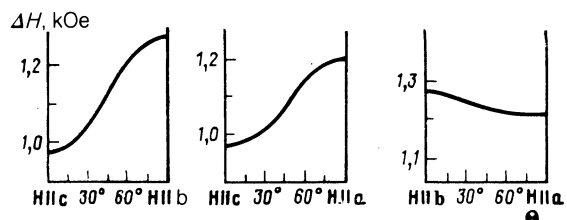


FIG. 8. Angular dependence of the EPR line width of the CuGeO_3 crystal.

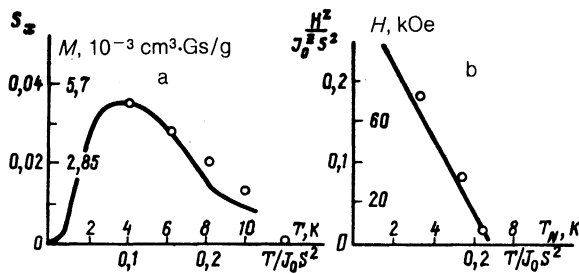


FIG. 9. Variation of the spontaneous magnetic moment, M , with temperature (a) and of the Néel temperature with applied magnetic field (b). Points show experimental data; the dashed curve is calculated by the Monte Carlo method for $J_2/J_0 = 0.8$ and $J_1/J_0 = 0.3$ (see text).

Our numerical calculations show that, upon introduction of a ferromagnetic bond $J_2 = 0.5J_1 > 0$ into the Hamiltonian (1), spins with frustrated J_1 bonds appear randomly in the system in such a way that there is no long-range magnetic order at $T = 0$. For $T \neq 0$, thermal spin oscillations are asymmetric. Furthermore, the average thermal value of transverse spin components becomes nonzero during the observation time, $\langle S_i^x \rangle \neq 0$.

One can use the susceptibility data (Fig. 4) to estimate the exchange-integral values of J_0 and of J_1 . The temperature T_{CW} where the susceptibility departs from the Curie-Weiss law and the temperature T_{χ_m} corresponding to the susceptibility maximum characterize these data. We calculate how these parameters vary with J_1/J_0 (see Fig. 10). Using the experimental curves of Fig. 4 and the calculated curve shown in Fig. 10a, it is possible to determine the value of J_1/J_0 . Furthermore, using the dependence shown in Fig. 10b we find the values of J_0 and J_1 . The values thus obtained from the susceptibility data along the b axis are: $J_0 = -430$ K, $J_1 = 64$ K, and $J_2 = 32$ K. A more precise determination of the exchange integrals requires susceptibility measurements for $T > 300$ K, since, as already mentioned, the region of temperature where $\chi^{-1}(T)$ is linear is very small (it is not observed at all for $\mathbf{H} \parallel \mathbf{c}$ orientations) and there is therefore a large error in the determined values of T_{CW} and of the paramagnetic Néel temperatures.

We now discuss the results of resonance measurements. As shown in Fig. 6, the EPR line width varies (linearly) strongly with temperature in the 30 K–300 K range. This implies a strong coupling between the magnetic system and thermal lattice vibrations. One of the possible mechanisms behind such behavior may be phonon modulation of the anisotropic exchange interaction.¹¹ Since the values of the paramagnetic Néel temperatures show large variations ($\Delta\Theta \sim 70$ K) as the orientation of the magnetic field changes, we can assume that the anisotropy contribution to the line width is large. Calculated values of $\Delta H(T)$, including the asymmetric Dzyaloshinskii-Moriya interaction $\mathbf{D}[\mathbf{S}_i \mathbf{S}_j]$, where \mathbf{D} is the Dzyaloshinskii-Moriya constant,¹⁰ exhibit similar behavior. The absence of inversion centers between Cu^{2+} ions placed along the CuGeO_3 crystal \mathbf{b} axis (see Fig. 2b) favors this mechanism.¹⁰ Analysis of the angular dependence of the line width $\Delta H(\theta)$ (see Fig. 8) allows

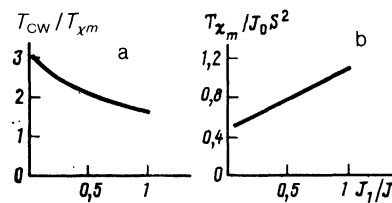


FIG. 10. Variation of T_{CW}/T_{χ_m} and of $T_{\chi_m}/J_0 S^2$ with J_1/J_0 , calculated by the Monte Carlo method.

us to conclude that phonon modulation of anisotropic exchange interaction is the main mechanism behind the temperature variation of the EPR line width.

It is also interesting to discuss the sharp change in magnetic and resonance properties of CuGeO_3 brought about by the amorphization process. The variations of the line width and of the resonant field with temperature change considerably. The small value of the paramagnetic temperature ($\Theta = -1.3$ K) for amorphous CuGeO_3 indicates a sharp drop of exchange interactions in the magnetic system studied. The CuGeO_3 crystal structure differs from that of other members of the AGeO_3 ($A = \text{Fe, Co, Mn}$) pyroxene family for which a spin glass state is found after the amorphization process.⁷ Unlike these other compounds, amorphous CuGeO_3 is paramagnetic down to 2 K, as shown by the susceptibility and EPR data. However, the observed resonance field dependence is typical of spin glasses, which leads us to believe that there is such a spin glass phase in amorphous CuGeO_3 but below a transition temperature of less than 2 K. Further studies, based on crystallographic data and properties of copper ions, of the differences in magnetic properties between amorphous AGeO_3 ($A = \text{Fe, Co, Mn}$) compounds and amorphous CuGeO_3 seem useful.

The authors thank N. I. Kiselev for temperature measurements of resistivity of the samples studied, A. E. Men'shikov for neutron diffraction measurements, and G. V. Losev for the differential thermal analysis of the samples.

¹E. V. Kuz'min, G. A. Petrakovskii, and S. S. Aplesnin, *J. Magn. Magn. Mat.* **15–18**, 1347 (1980).

²G. A. Petrakovskii and S. S. Aplesnin, *Phys. Status Solidi B* **117**, 401 (1983).

³G. A. Petrakovskii, *Usp. Fiz. Nauk* **134**, 305 (1981) [*Sov. Phys. Usp.* **24**, 511 (1981)].

⁴G. A. Petrakovskii, K. A. Sablina, V. E. Volkov, Yu. M. Fedorov, I. M. Stolovitskii, V. I. Chechernikov, and V. L. Yakovenko, *Zh. Eksp. Teor. Fiz.* **85**, 592 (1983) [*Sov. Phys. JETP* **58**, 345 (1983)].

⁵G. A. Petrakovskii, K. A. Sablina, V. P. Ikonnikov, I. A. Volkov, and A. G. Klimenko, *Phys. Status Solidi A* **70**, 507 (1982).

⁶G. A. Petrakovskii, K. A. Sablina, and V. P. Ikonnikov, *Phys. Status Solidi A* **75**, K165 (1983).

⁷G. A. Petrakovskii, K. A. Sablina, and A. G. Klimenko, *Proceedings of International Conference on Physics of Transition Metals*, Kiev, 1988, p. 61.

⁸Y. Ginetti, *Bull. Soc. Chim. Belg.* **63**, 209 (1954).

⁹*Handbook on Physical and Chemical Properties of Oxides*, Metallurgiya, 1978.

¹⁰T. Moriya, *Phys. Rev.* **120**, 91 (1960).

¹¹M. S. Seehra and T. G. Castner, *Phys. Condens. Mater.* **7**, 185 (1968).

Translated by Jolanta Stankiewicz